

Disordered weak and strong topological insulators

Koji Kobayashi¹, Tomi Ohtsuki¹, and Ken-Ichiro Imura²

¹*Department of Physics, Sophia University, Tokyo Chiyoda-ku 102-8554, Japan and*

²*Department of Quantum Matter, AdSM, Hiroshima University, Higashi-Hiroshima 739-8530, Japan*

(Dated: October 18, 2012)

Robustness against disorder is a defining property of the topological quantum phenomena. Here, we highlight unexpected robustness of transport characteristics found in a lattice model of disordered three-dimensional \mathbb{Z}_2 topological insulator. We have studied numerically the global phase diagram of this model yielding both the weak and strong topological insulator (WTI and STI) phases to quantify how they collapse as a function of disorder. We have found that the average two-terminal conductance is quantized both in the bulk and slab geometries. This indicates that not only the surface Dirac cones in the STI and WTI phases but also bulk Dirac cones emergent at the phase boundaries exhibit robustness against disorder. We have also studied the Lyapunov exponents in the quasi one-dimensional geometry to verify that both the STI and WTI phases are indeed stable up to a finite strength of disorder.

PACS numbers: 73.20.-r, 73.20.Fz, 71.23.-k, 71.30.+h

The \mathbb{Z}_2 topological insulator [1–3] is a time-reversal invariant counterpart of the quantum Hall state. The former realizes due to spin-orbit coupling preserving the time reversal symmetry (TRS), while the latter occurs under a strong magnetic field breaking the TRS. As the quantum Hall state is characterized by an integral (\mathbb{Z} -type) topological invariant (Chern number), the \mathbb{Z}_2 topological insulator is distinguished from “ordinary” insulators (OI) by an analogous \mathbb{Z}_2 topological number, taking only two possible values: 0 and 1. For three-dimensional (3D) \mathbb{Z}_2 topological insulators, there exist four of such \mathbb{Z}_2 topological invariants [4–6] implying the existence of the so-called strong and weak topological insulators (STI and WTI) [7]. Here, the term “strong” or “weak” is prescribed by the robustness of the state against perturbations that preserve the system’s underlying TRS. Though WTI is *a priori* considered weak, it is definitely an open issue both theoretically and experimentally to quantify how weak the WTI actually is against disorder [8, 9]. This should be naturally discussed in the light of how robust the STI is in the presence of disorder. In the following we address these issues by studying numerically the global phase diagram of such a 3D disordered \mathbb{Z}_2 topological insulator implemented on a lattice employing the transfer matrix method.

Topological insulators are characterized by a bulk topological invariant encoding their nontrivial band structure, but through the bulk/surface correspondence this is equivalent to say that they exhibit topologically protected gapless surface states. While an STI exhibits a single helical Dirac cone that is protected, a WTI manifests generally an even number of Dirac cones that can be null depending on the orientation of the surface [7]. In the study of graphene, the unusual robustness of Dirac electrons (especially in the case of a single Dirac cone) against disorder has been widely recognized. As a consequence of the absence of backward scattering [10], the Dirac electrons do not localize [11, 12]. However, in the

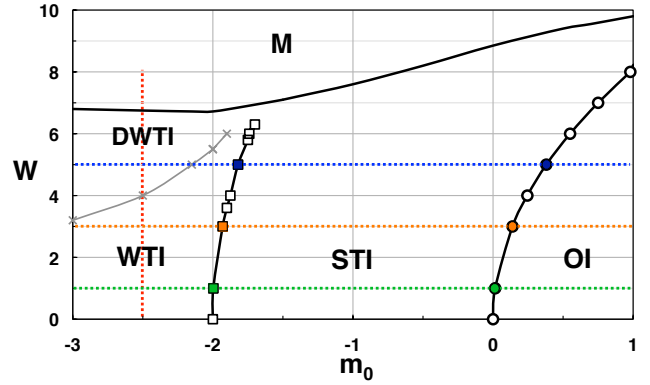


FIG. 1: (Color online) The “global phase diagram” of disordered \mathbb{Z}_2 topological insulator in the (m_0, W) -plane determined by the behavior of two-terminal conductance. Solid lines on the phase boundaries are guides to the eyes. Dotted lines indicate the value of parameters relevant in Figs. 2 and 3. Metallic (M) phase lies in the intermediate range of disorder strength, typically $10 \lesssim W \lesssim 25$ in the parameter range of m_0 shown in this figure.

presence of valleys (even number of Dirac cones) as in the case of graphene, they do localize mediated by inter-valley scatterings [13]. Does this mean that an STI continues to be an STI for an arbitrary strength of short-ranged potential disorder that induces an inter-valley scattering, while a WTI simply collapses on switching on of the disorder? The reality is quite different from this naive speculation as shown in the phase diagram depicted in Fig. 1. This phase diagram established by a combination of the study of the averaged two-terminal conductance and of the quasi-1D decay length in the transfer matrix approach is intended to sketch the main results of the paper. In the phase diagram m_0 is the magnitude of the bulk energy gap at the Γ point (when m_0 is negative, the gap is inverted), while W is the strength of disorder. Notice also that in the model employed [see Eq. (1)], a

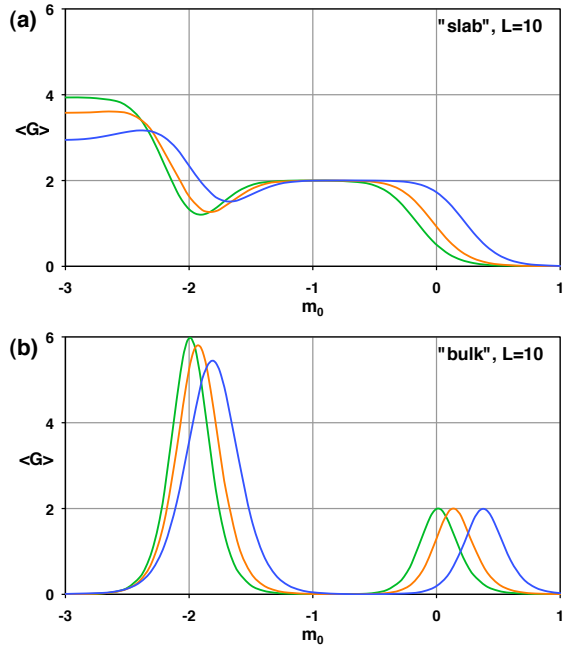


FIG. 2: Two-terminal conductance $\langle G \rangle$ (a) in the slab and (b) in the bulk geometries. $\langle G \rangle$ is plotted against m_0 for a system of size $L = 10$ under different strength of disorder: $W = 1$ (green), $W = 3$ (red), and $W = 5$ (blue). In the bulk geometry PBC's are imposed in both the x - and y -directions, while in the slab geometry, FBC is applied to the x -direction.

WTI phase with weak indices [7] $(\nu_0, \nu_1 \nu_2 \nu_3) = (0, 111)$ appears in the regime: $-4 < m_0 < -2$. The entire phase diagram is symmetric with respect to $m_0 = -3$. To identify the nature of different phases and the location of the phase boundaries in the (m_0, W) -plane, use of different geometries (i.e., bulk vs. slab) is shown to be crucial. While a plateau of the conductance in the slab geometry characterizes the nature of the corresponding phase [e.g., Fig. 2(a)], the phase boundaries are marked by a peak of the conductance in the bulk geometry [e.g., Fig. 2(b)]. Under the breaking of translational invariance by disorder, standard techniques [7] for calculating the topological invariants fail. Yet, the above behaviors of the conductance clearly distinguish different topological phases, providing us with sufficient information for establishing the phase diagram depicted in Fig. 1.

Let us begin by pointing out that both STI and WTI phases in the clean limit ($W = 0$) survive in the presence of finite disorder, but collapse into a metallic phase (the M-phase in Fig. 1) at a certain strength of disorder. We have confirmed the robustness of these insulating phases by studying the system size dependence of the average conductance $\langle G \rangle$. The existence of surface helical Dirac cones and their nature are revealed by studying the generalized quasi-1D decay length ξ_i .

As for the global structure of the phase diagram, note that the STI exhibits a direct boundary with the OI phase [14], without being intervened by an extension of the

symplectic metal phase [15]. This is quite contrary to the case of the phase diagram for the 2D version of our model [16, 17]. In the weakly disordered regime, a couple of marked features are to be mentioned. First the WTI phase has an internal structure; it is divided into WTI and defeated WTI (DWTI) regions, reflecting the change of the system size dependence of the conductance. This indicates that a WTI phase is in a sense indeed weak compared with the STI. We leave detailed description of the DWTI region to the second half of the paper. Another remarkable feature in this regime is the shape of the phase boundaries between different insulating phases. The positions of these phase boundaries are determined by the behavior of average conductance in the bulk and in the slab geometries (see Fig. 2). In the case of STI/OI boundary, a gradual shift of this position (to the OI side) as increasing disorder represents a feature often referred to as a “topological Anderson insulator” [18–20]. A similar gradual shift of the phase boundary can be also seen at the WTI/STI boundary. On this side of the phase, the STI turns out to be less expansive, invaded by the WTI. This tendency of the phase boundary is consistent with the SCBA calculation [21].

Another unexpected feature we found in this study is the quantization of the peak conductance at the phase boundaries [see, e.g., Fig. 2(a)]. At the phase boundary, the bulk energy gap closes and in the model studied 3D Dirac cones emerge in the spectrum, dominating the transport characteristics of the system. The number of such Dirac cones is 1 at the STI/OI boundary, while it is 3 at the WTI/STI boundary. As can be seen in Fig. 2(a), the height of the conductance peak is approximately given by twice this number in units of e^2/h , i.e., $G = 2$ at the STI/OI boundary, and $G = 6$ at the WTI/STI boundary. This is because a 3D bulk Dirac cone gives rise to two 1D channels in the vicinity of $E = 0$. By studying the size dependence of G , we have verified that the height of the peak value of G approaches indeed the quantized value, given by twice the number of Dirac cones. The quantization is an indication of a certain degree of robustness of the 3D Dirac cones against disorder. We mention that the fluctuation of G is strongly suppressed as approaching the peak. This is in contrast to the quantum (spin) Hall transition, where a finite universal fluctuation is observed [22].

As a concrete implementation of a 3D \mathbb{Z}_2 topological insulator on a lattice, we consider the following Wilson-Dirac type tight-binding Hamiltonian [23, 24],

$$H = \sum_{\mathbf{x}} \sum_{k=x,y,z} \left[\frac{it}{2} c_{\mathbf{x}+\mathbf{e}_k}^\dagger \alpha_k c_{\mathbf{x}} - \frac{r}{2} c_{\mathbf{x}+\mathbf{e}_k}^\dagger \beta c_{\mathbf{x}} + \text{h.c.} \right] + (m_0 + 3r) \sum_{\mathbf{x}} c_{\mathbf{x}}^\dagger \beta c_{\mathbf{x}} + \sum_{\mathbf{x}} v_{\mathbf{x}} c_{\mathbf{x}}^\dagger 1_4 c_{\mathbf{x}}, \quad (1)$$

where $c_{\mathbf{x}}^\dagger$ and $c_{\mathbf{x}}$ are creation and annihilation operators on a site \mathbf{x} , \mathbf{e}_k is a unit vector, α_k and β are gamma

matrices in the Dirac representation

$$\alpha_k = \begin{pmatrix} 0 & \sigma_k \\ \sigma_k & 0 \end{pmatrix}, \quad \beta = \begin{pmatrix} 1_2 & 0 \\ 0 & -1_2 \end{pmatrix}, \quad (2)$$

where σ_k are Pauli matrices and 1_2 is 2×2 identity matrix, t, r, m_0 are parameters, and disorder potential v_x are uniformly distributed between $-W/2$ and $W/2$. We set $r = 1, t = 2$, as in Ref. [24]. This Hamiltonian belongs to the symmetry class AII [25] (or, DIII for $W = 0$).

The transfer matrix [26, 27] is given in terms of the wave function ψ_n on a slice at $z = n$ as

$$\begin{pmatrix} \psi_{n+1} \\ H_+ \psi_n \end{pmatrix} = T_n \begin{pmatrix} \psi_n \\ H_+ \psi_{n-1} \end{pmatrix}, \quad T_n = \begin{pmatrix} -H_-^{-1} H_n & -H_-^{-1} \\ H_+ & 0 \end{pmatrix},$$

where $H_n = \langle n | H | n \rangle - E$, $H_- = \langle n | H | n+1 \rangle$ and $H_+ = \langle n+1 | H | n \rangle$. We set $E = 0$ in this study, though similar results are obtained for $E = 0.05$.

To determine the phase boundaries between different insulating phases, we calculate the (average) two-terminal conductance, using the Landauer formula [22]. The transport between the left and right terminals is described in terms of the scattering matrix S defined as

$$\begin{pmatrix} \psi_L^{\text{out}} \\ \psi_R^{\text{out}} \end{pmatrix} = S \begin{pmatrix} \psi_L^{\text{in}} \\ \psi_R^{\text{in}} \end{pmatrix}, \quad S = \begin{pmatrix} r & t' \\ t & r' \end{pmatrix}, \quad (3)$$

where $\psi_{L(R)}^{\text{in(out)}}$ denotes the incoming (outgoing) state on the left (right) terminal, and t and t' (r and r') are transmission (reflection) matrices. The conductance G in units of e^2/h is given by $G = \text{Tr}(t^\dagger t)$. To find the explicit form of the S -matrix, we employ a transfer matrix for a system of length L . The actual computation has been done in a cubic geometry of $L \times L \times L$ sites with electrodes attached to the z -direction. We assume that the electrodes consist of L^2 perfectly-conducting 1D wires as in network models [22], so that details of the electrodes do not affect the conductance.

Typical examples of the calculated conductance curves are shown in Fig. 2. In the upper panel (a) the conductance is calculated in the “slab” geometry, i.e., fixed boundary condition (FBC) in the x -direction and periodic boundary condition (PBC) in y -direction (note z -direction is the direction of transport). In the lower panel (b), PBC’s are imposed in both the x - and y -directions (“bulk” geometry). The conductance is indeed very sensitive to the change of these boundary conditions. In the slab geometry, on the contrary, the conductance shows a plateau behavior, also quantized at $\langle G \rangle = 2$ in the STI, and at $\langle G \rangle \simeq 4$ in the WTI phases. In the bulk geometry, the conductance exhibits a sharp peak feature at the phase boundary between different insulating phases, while inside the insulating phases, irrespective of their topological non-triviality (either in the STI, WTI, or OI phases), the conductance tends to vanish in the thermodynamic limit. Note that if one considers the robustness

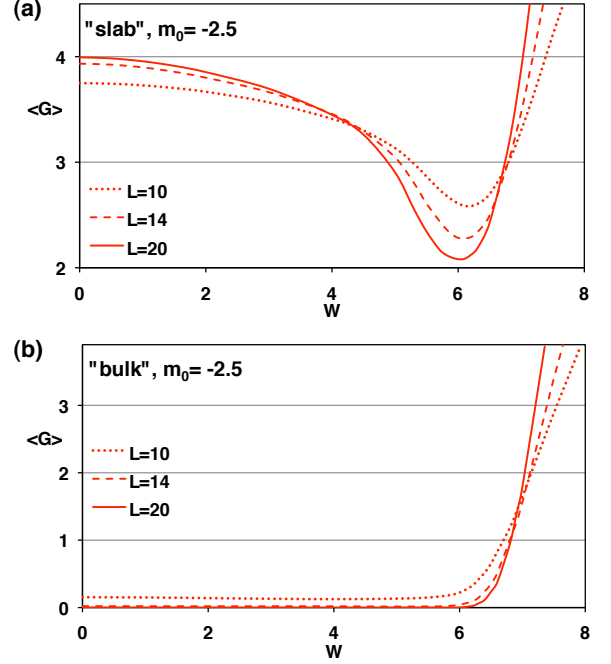


FIG. 3: Two-terminal conductance as a function of disorder with $m_0 = -2.5$ for different system sizes: $L = 10$ (dotted), $L = 14$ (dashed), and $L = 20$ (solid). The upper panel (a) is for the slab geometry. The weak topological surface states are stable for a certain value of disorder (about $W \lesssim 4$, which is actually not small), and defeated by disorder around $W = 6.0$. For $W \gtrsim 7$, the system enters metallic phase. The lower panel (b) shows the conductance in bulk geometry. There are no peak that should appear at the topological phase transition point around $W \simeq 4$. The statistical error is less than 0.02.

of the helical surface Dirac cones (or, at least of a single Dirac cone) emergent on the surface of a slab, quantization of these conductance plateaus is an expected behavior up to a different degree of the quantization in the STI and WTI phases. In contrast, apparent quantization of the height of conductance peaks in the bulk geometry [Fig. 2(a)] was unexpected, since this quantization stems from the bulk Dirac cones. The positions of the conductance peaks show little dependence on L and have been used to determine the phase boundaries of Fig. 1.

To reinforce the validity of the phase diagram, we have also studied the Lyapunov exponents in the quasi-one-dimensional geometry. A Lyapunov exponent γ_i is defined as

$$\gamma_i = \lim_{M \rightarrow \infty} \frac{\ln \lambda_i}{2M}, \quad (4)$$

where λ_i is a positive eigenvalue of the matrix $\mathcal{T}^\dagger \mathcal{T}$, and $\mathcal{T} = T_M \cdots T_2 T_1$ is a product of the M transfer matrices of dimension $8L_x L_y$ [26]. Due to the current conservation, λ_i occurs in reciprocal pairs and due to the Kramers degeneracy, they are doubly degenerate. Keeping this in mind, we arrange the exponents in the decreasing order, $\gamma_{2L_x L_y} > \gamma_{2L_x L_y - 1} > \cdots > \gamma_2 > \gamma_1 > 0 > -\gamma_1 > \cdots >$

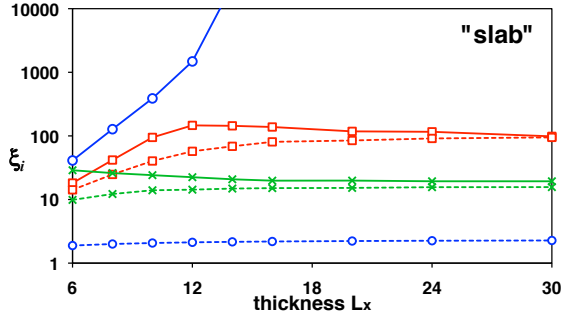


FIG. 4: (Color online) Decay lengths ξ_1 (solid lines) and ξ_2 (dashed lines) in the STI $(m_0, W) = (-1, 1)$ (blue \circ), the WTI $(m_0, W) = (-2.5, 3.5)$ (red \square), and DWTI $(m_0, W) = (-2.5, 6)$ (green \times) regions in the slab geometry with system width $L_y = 6$. The error bars are less than 5%.

$-\gamma_2 L_x L_y$. The smallest positive Lyapunov exponent γ_1 is identified as the quasi-1D decay length ξ by the correspondence, $\xi = 1/\gamma_1$. Here, we extend this to higher Lyapunov exponents [28, 29]:

$$\xi_i = \frac{1}{\gamma_i}. \quad (5)$$

In the metallic phase, all the generalized decay length ξ_i 's uniformly increase as functions of the size of the cross section L_x and L_y . In the OI phase, the decay lengths are insensitive to L_x and L_y . In the topological insulating phases with slab geometry, higher decay lengths behave similarly to those of the OI phase, while the behavior of the largest few ξ_i 's is clearly distinguishable from those of the OI phase. They are significantly large, but in contrast to the metallic states, they show specific dependence on the system's thickness L_x . These behaviors reflect the nature of the 2D surface states. Indeed, the number of these special ξ_i 's corresponds to the number of Dirac cones on a surface (1 for STI and 2 for WTI).

Let us carefully see the transport properties of the STI and WTI phases (in Fig. 1) in the presence of disorder by using the conductance and decay length. In the STI phase, the conductance approaches the quantized value $G = 2$ irrespective of the disorder strength, and form a conductance plateau [see Fig. 2(a)]. In this plateau region, the largest decay length ξ_1 increases rapidly (exponentially) with L_x (see, e.g., Fig. 4), while the others $\xi_{i \geq 2}$ are of the same order of ξ_i 's for ordinary insulators. This implies that there is a single robust Dirac cone on each surface and in the limit $L_x \rightarrow \infty$, it becomes perfectly conducting (*cf.* systems of an odd number of channels, see Ref. [30, 31]). We have noticed that the dependence of ξ_i on the system's width L_y is notably complicated. As L_y increases, higher order ξ_i 's start to exhibit a non-monotonic dependence. The number of such anomalous ξ_i 's increases with the increase of L_y in a certain interval of L_y , and each time this number changes by two per Dirac cone. Presumably, this is caused by opening of

higher subbands of the helical Dirac cones as a 1D channel separated from the bulk bands. Thus in the thermodynamic limit $L_x, L_y, L_z \rightarrow \infty$, the conductance may become infinite, instead of taking a quantized value.

In the WTI phase, we have found that there are two regions where the conductance shows different dependence on the cube size L . For weak disorder ($W \lesssim 4$ for $m_0 = -2.5$), the conductance increases and asymptotically approaches a finite value $G \simeq 4$ as L increases [see Fig. 3(a)]. In this weakly disordered regime, the decay lengths ξ_1 and ξ_2 tend to increase as ξ_1 in the STI phase, before being saturated as L_x increases (see Fig. 4) at a value *ca.* 50 times larger than ξ_3 . The saturation of ξ is caused by a small but finite inter-valley scattering amplitude, which was absent in the STI phase. Combining these two observations, one can convince oneself that the surface states of a WTI indeed remain stable in this regime of a finite disorder strength. On the contrary, once the disorder exceeds a certain value ($W \simeq 4$), the conductance decays with increasing L (Fig. 3) and ξ_1 and ξ_2 do not show an exponential rise. Such a behavior is indeed indistinguishable from the case of OI. What is then the nature of these two regimes, WTI and DWTI in Fig. 1? Are they distinct phases, and is there a transition between the two? Our result suggests the following. The absence of a conductance peak between the WTI and DWTI regions [see Fig. 3(b)] implies that they are topologically identical. Actually, ξ_1 and ξ_2 , which correspond to the surface states, are still large and distinguishable from the bulk states (although they are smaller than those in the STI and WTI phases). In the DWTI region, surface conducting states are simply "defeated" by disorder. In this sense we name this region the defeated WTI or DWTI region. The fate of the WTI and DWTI regions in thermodynamic limit is highly nontrivial. We leave more substantial presentation on this point to a forthcoming publication.

We have seen in this paper that the surface states of a WTI exhibit unexpected robustness, but are defeated by a sufficient strength of disorder. It is also shown that a single helical Dirac cone on the surface of an STI is not unrivaled. In the lattice model studied, it collapses under a finite strength of disorder, just as in the case of WTI surface states. Disorder can also drive an STI into a WTI. We have proposed that topologically non-trivial phases in the presence of disorder can be characterized by the number of the (generalized) decay length ξ_i that is significantly larger than the bulk decay length. Typically, this number is 1 for STI and 2 for WTI/DWTI.

This work was supported by KAKENHI No. 23-3743, No. 23540376, and No. 23103511. The authors thank Y. Takane, K. Nomura, K. Slevin, A. Yamakage, and R. Shindou for useful discussions.

-
- [1] B. A. Bernevig, T. L. Hughes, and S. C. Zhang, *Science* **314**, 1757 (2006).
- [2] M. Z. Hasan and C. L. Kane, *Rev. Mod. Phys.* **82**, 3045 (2010).
- [3] X.-L. Qi and S.-C. Zhang, *Rev. Mod. Phys.* **83**, 1057 (2011).
- [4] L. Fu, C. L. Kane, and E. J. Mele, *Phys. Rev. Lett.* **98**, 106803 (2007).
- [5] J. E. Moore and L. Balents, *Phys. Rev. B* **75**, 121306(R) (2007).
- [6] R. Roy, *Phys. Rev. B* **79**, 195322 (2009).
- [7] L. Fu and C. L. Kane, *Phys. Rev. B* **76**, 045302 (2007).
- [8] R. S. K. Mong, J. H. Bardarson, and J. E. Moore, *Phys. Rev. Lett.* **108**, 076804 (2012).
- [9] Z. Ringel, Y. E. Kraus, and A. Stern, *Phys. Rev. B* **86**, 045102 (2012).
- [10] T. Ando, T. Nakanishi, and R. Saito, *J. Phys. Soc. Jpn.* **67**, 2857 (1998).
- [11] K. Nomura, M. Koshino, and S. Ryu, *Phys. Rev. Lett.* **99**, 146806 (2007).
- [12] J. H. Bardarson, J. Tworzydło, P. W. Brouwer, and C. W. J. Beenakker, *Phys. Rev. Lett.* **99**, 106801 (2007).
- [13] H. Suzuura and T. Ando, *Phys. Rev. Lett.* **89**, 266603 (2002).
- [14] R. Shindou and S. Murakami, *Phys. Rev. B* **79**, 045321 (2009).
- [15] S. Hikami, A. I. Larkin, and Y. Nagaoka, *Prog. Theor. Phys.* **63**, 707 (1980).
- [16] A. Yamakage, K. Nomura, K.-I. Imura, and Y. Kuramoto, *J. Phys. Soc. Jpn.* **80**, 053703 (2011).
- [17] E. Prodan, *Phys. Rev. B* **83**, 195119 (2011).
- [18] J. Li, R.-L. Chu, J. K. Jain, and S.-Q. Shen, *Phys. Rev. Lett.* **102**, 136806 (2009).
- [19] C. W. Groth, M. Wimmer, A. R. Akhmerov, J. Tworzydło, and C. W. J. Beenakker, *Phys. Rev. Lett.* **103**, 196805 (2009).
- [20] H.-M. Guo, G. Rosenberg, G. Refael, and M. Franz, *Phys. Rev. Lett.* **105**, 216601 (2010).
- [21] A. Yamakage, private communication.
- [22] K. Kobayashi, T. Ohtsuki, H. Obuse, and K. Slevin, *PRB* **82**, 165301 (2010).
- [23] X.-L. Qi, T. L. Hughes, and S.-C. Zhang, *Phys. Rev. B* **78**, 195424 (2008).
- [24] S. Ryu and K. Nomura, *Phys. Rev. B* **85**, 155138 (2012).
- [25] M. R. Zirnbauer, *J. Math. Phys.* **37**, 4986 (1996).
- [26] A. MacKinnon and B. Kramer, *Z. Phys. B* **53**, 1 (1983).
- [27] A. Eilmes, A. M. Fischer, and R. A. Römer, *Phys. Rev. B* **77**, 245117 (2008).
- [28] K. Slevin and T. Ohtsuki, *Phys. Rev. B* **63**, 045108 (2001).
- [29] K. Kobayashi, T. Ohtsuki, and K. Slevin, *IJMPCS* **11**, 114 (2012).
- [30] Y. Takane, *J. Phys. Soc. Jpn.* **73**, 2366 (2004).
- [31] K. Kobayashi, K. Hirose, H. Obuse, T. Ohtsuki, and K. Slevin, *J. Phys.: Conf. Ser.* **150**, 022041 (2009).